Elemental and cooperative diffusion in a liquid, supercooled liquid and glass resolved

Daniel R. Cassar, Ricardo F. Lancelotti, Rafael Nuernberg, Marcio L. F. Nascimento, Alisson M. Rodrigues, Luiza T. Diz, and Edgar D. Zanotto

Elemental and cooperative diffusion in a liquid, supercooled liquid and glass resolved

Daniel R. Cassar,[1,a),b)] Ricardo F. Lancelotti,[1,b)] Rafael Nuernberg,[1,b)]
Marcio L. F. Nascimento,[2,c)] Alisson M. Rodrigues,[1,b)] Luiza T. Diz,[1,b)]
and Edgar D. Zanotto[1,a),b)]

[1]*CeRTEV—Center for Research, Technology and Education in Vitreous Materials, Department of Materials Engineering, Federal University of São Carlos, 13565-905 São Carlos, SP, Brazil*
[2]*PROTEC/PEI—Graduate Program in Industrial Engineering, Department of Chemical Engineering, Polytechnic School, Federal University of Bahia, Rua Aristides Novis 2, Federação, 40210-630 Salvador, BA, Brazil*

The diffusion mechanisms controlling viscous flow, structural relaxation, liquid-liquid phase separation, crystal nucleation, and crystal growth in multicomponent glass-forming liquids are of great interest and relevance in physics, chemistry, materials, and glass science. However, the diffusing entities that control each of these important dynamic processes are still unknown. The main objective of this work is to shed some light on this mystery, advancing the knowledge on this phenomenon. For that matter, we measured the crystal growth rates, the viscosity, and lead diffusivities in $PbSiO_3$ liquid and glass in a wide temperature range. We compared our measured values with published data covering 16 orders of magnitude. We suggest that above a certain temperature range T_d ($1.2T_g$–$1.3T_g$), crystal growth and viscous flow are controlled by the diffusion of silicon and lead. Below this temperature, crystal growth and viscous flow are more sluggish than the diffusion of silicon and lead. Therefore, T_d marks the temperature where *decoupling* between the (measured) cationic diffusivity and the effective diffusivities calculated from viscosity and crystal growth rates occurs. We reasonably propose that the nature or size of the diffusional entities controlling viscous flow and crystal growth below T_d is quite *different*; the slowest is the one controlling viscous flow, but *both* processes require cooperative movements of some larger structural units rather than jumps of only one or a few isolated atoms. *Published by AIP Publishing.* [http://dx.doi.org/10.1063/1.4986507]

I. INTRODUCTION

The diffusion mechanisms controlling key dynamic processes—viscous flow, structural relaxation, liquid-liquid phase separation, crystal nucleation, and crystal growth—in complex glass-forming supercooled liquids, such as silicate melts, have been a matter of great interest and relevance in the physics, chemistry, and materials science fields for many decades. However, the atomic entities (structural units) that dominate and control each one of these processes are still unknown. These structural units could be individual network forming ions (such as oxygen and silicon) or a more complex unit involving one or more SiO_4 tetrahedra. In theory, this entity could even include network modifier cations.

One well established phenomenon regarding dynamic processes in glass-forming liquids is the so-called *breakdown* of the Stokes–Einstein–Eyring (SEE) equation.[1] Briefly, this is a decoupling phenomenon between crystal growth and viscous flow kinetics that occurs below a certain temperature, the so-called *decoupling temperature*, T_d, observed in

the range of 1.1–$1.3T_g$. T_g is the laboratory glass transition temperature,[2,3] usually taken as the temperature where the equilibrium viscosity reaches 10^{12} Pa s. Below T_d, the *nature* or *size* of the diffusing species that control these two kinetic processes is clearly different. However, as we already stressed, the details about these species are still unknown. To the best of our knowledge, it is *only* in the case of the strong glass former SiO_2 that the decoupling phenomenon has not been detected. In this liquid, self-diffusion of Si^{4+} and O^{2-} controls both the viscous flow and crystal growth rates[4] all the way from above the melting point down to T_g.

A relevant article which is well within the scope of this work is that of Farnan and Stebbins.[5] These authors carried out a series of *in situ* high-temperature 2D-NMR experiments for $K_2Si_4O_9$. They showed experimentally that the time scale of local silicate species exchange, between the Q^3 and Q^4 species, in this composition was the same as that of the shear relaxation time.[5] As the characteristic shear relaxation time, τ, is directly related to the equilibrium viscosity, η ($\tau = \eta/G_\infty$, where G_∞ is the infinite frequency elastic shear modulus), this proposed mechanism is contrary to the widespread accepted assumption that *cooperative movements* of some "structural units" control viscous flow in glass-forming liquids. The flow mechanism appeared to involve a change in the nature of oxygen in the liquid between bridging (BO) and non-bridging (NBO) roles.

a)Authors to whom correspondence should be addressed: daniel.r.cassar@gmail.com and dedz@ufscar.br
b)URL: www.certev.ufscar.br.
c)URL: www.protec.ufba.br.

According to Farnan,[6] this is equivalent to a change in local silicate species. Hence Stebbins proposed that the Q species exchange is closely related to the mechanism of viscous flow.[7] He also suggested that if viscous flow is closely linked to the rate of network bond breaking, then it should also be closely related to the diffusivities of the network forming cations and anions.

In this paper, we focus on the lead metasilicate composition ($PbSiO_3$, abbreviated as PS). To the best of our knowledge, apart from pure SiO_2, PS is the only other known stoichiometric oxide glass-forming composition for which experimentally measured diffusion coefficients of network former cations (silicon and lead) are available in a wide temperature range,[8–10] above and below T_g. The diffusivities of silicon and/or oxygen species could be used as proxies of melt viscosity in silicate systems.[7] Our main objective is to compute the diffusion coefficients controlling *viscous flow* and *crystal growth* and compare them with published self-diffusion data of Si and Pb for lead metasilicate in the liquid, supercooled liquid, and glassy states. This is an attempt to understand the mechanisms controlling these two important kinetic processes. We hope that this comparison might shed some light on whether *elemental diffusion* or *cooperative rearrangements* of some larger structural units control viscous flow and crystal growth.

II. LITERATURE REVIEW

A. Structure of $PbSiO_3$ glass

The structure of lead metasilicate glass has been extensively studied using different spectroscopic techniques,[11–14] neutron and X-ray diffraction.[15] Lee and Kim[14] studied lead silicate glasses (with lower SiO_2 content than $PbSiO_3$) and observed that the mixing between Si and Pb deviates from a random distribution. It has been shown by NMR that Q^2 (40%–60%), Q^3 (25%–35%), and Q^4 (6%) units are predominant in this material with very low fractions of Q^0+Q^1. In another study,[13] only Q^2 and Q^4 were predicted by thermodynamic modeling in this glass. All these results indicate an unbalanced Q^n distribution toward glass-forming units (Q^3+Q^4). In a study using high-energy X-ray and neutron diffraction measurements and structural modeling, Kohara *et al.*[15] concluded that $PbSiO_3$ can be categorized as a dual network-former glass. Besides, they claim that the formation of the network is governed by the interplay of SiO_4 tetrahedra and PbO_x polyhedra as network forming units, which results in a glass with an unusual amount of free volume (void space) that is not observed in other binary systems, such as $CaO-SiO_2$ and Na_2O-SiO_2. Hence, a fraction of the Pb^{2+} ions indeed play the role of network formers.

It is relevant to mention an experimental fact that corroborates the dual network former concept; $PbO \cdot SiO_2$ is likely to be the only *metasilicate* glass that shows a very good glass-forming ability as it easily vitrifies on the cooling path from the liquid state without any signs of crystallization even at low cooling rates. In contrast, for instance, other metasilicates, $Li_2O \cdot SiO_2$, $Na_2O \cdot SiO_2$, $MgO \cdot SiO_2$, and $BaO \cdot SiO_2$, are very reluctant glass formers.

B. Crystal growth

Nascimento and co-authors[3] have studied the temperature dependence of crystal growth rates in several supercooled liquids, including lead metasilicate. They have tested several growth models and considered that the secondary superficial nucleation growth mechanism (also known as "2D growth") describes the experimental growth rates well for lead metasilicate[16] for temperatures above $T_d \sim 1.3 T_g$.

Equation (1) shows the general formula for this growth mechanism. In this equation, parameters B and C depend on the secondary crystal nucleation rate that occurs at the interface between a primary crystal and the ambient phase. If this rate is sufficiently small then one has the layer-by-layer case scenario (also known as "small crystal case"), with B equal to one and C given by Eq. (2). However, if this rate is sufficiently large, the polynuclei case scenario dominates (also known as "large crystal case"), with B equal to 3 and C given by Eq. (3).

$$U = C \frac{D_U}{d_0^2} \exp\left(-\frac{\pi d_0 \gamma^2}{B k_B T \Delta\mu_V}\right), \tag{1}$$

$$C = d_0 N_S A_0, \tag{2}$$

$$C = \frac{1}{\Gamma(4/3)} \sqrt[3]{\frac{\pi N_S d_0^5}{3}} \left[1 - \exp\left(-\frac{\Delta\mu}{RT}\right)\right]^{\frac{2}{3}}. \tag{3}$$

In the above equations, U is the crystal growth rate; D_U is the effective diffusion coefficient of the structural units that take part in crystal growth; d_0 is their size; γ is the interfacial energy between the crystal and the supercooled liquid; k_B is the Boltzmann constant; T is the absolute temperature; $\Delta\mu_V$ is the driving force for crystallization per unit volume [see Eq. (4) [17,18]]; N_S is the number of possible nucleation sites per unit area; A_0 is the critical area of a secondary nucleus at the crystal interface; Γ is the gamma function; $\Delta\mu$ is the driving force for crystallization per mole [see Eq. (5) below]; and R is the gas constant.

The driving force for crystallization is given by Eqs. (4) and (5),

$$\Delta\mu_V = \frac{\Delta\mu}{V_m}, \tag{4}$$

$$\Delta\mu = \Delta H_m \left(1 - \frac{T}{T_m}\right) - \int_T^{T_m} (C_{p,l} - C_{p,c}) dT + T \int_T^{T_m} \frac{C_{p,l} - C_{p,c}}{T} dT. \tag{5}$$

Here, V_m is the molar volume; ΔH_m is the melting enthalpy; T_m is the melting temperature; and C_p is the molar heat capacity. The subscripts "l" and "c" refer to the liquid and the crystalline phases, respectively.

We calculated V_m and N_S using d_0, as shown below and used the A_0 expression deduced by Cassar.[19] The deduction is reproduced in the Appendix. N_A is the Avogadro's number.

$$V_m = d_0^3 N_A, \tag{6}$$

$$N_S = \left(\frac{1}{d_0}\right)^2, \tag{7}$$

$$A_0 = \frac{2\pi\gamma d_0}{\Delta\mu_V}. \tag{8}$$

C. Diffusion

As we mentioned in the Introduction, measured *self-diffusion coefficients* for silicon (D_{Si}) and lead (D_{Pb}) ions[8–10] are available for lead metasilicate liquid, supercooled liquid, and glass. Here we extend the range of available D_{Pb} using impedance measurements and the Nernst–Einstein relation,

$$D_\sigma = \frac{\sigma k_B T}{e^2 N_i}, \qquad (9)$$

where N_i is the number density of mobile ions, e is the elemental charge, and σ is the conductivity.

In Eq. (9), the number density of Pb ions can be estimated from the glass density and composition. However, it is important to note that D_σ is not a diffusion coefficient that can be calculated or explained by Fick's laws. The ratio between tracer diffusivity (D_t) and charge diffusivity (D_σ) is known as the Haven ratio ($H_r = D_t/D_\sigma$) and gives information about the correlation between tracer and charge diffusivities related to the atomic mechanism of ionic motion.

For the *interstitial diffusion* mechanism in *crystals*, where the current is due to the drift of interstitial ions under an applied field, D_t and D_σ are equal, resulting in a Haven ratio of 1. For the *vacancy diffusion* mechanism in *crystals*, the charge is effectively carried by the vacancies, giving a D_t that depends on the ion-ion coordination number, and is not equal to D_σ. For the *vacancy diffusion* mechanism in *glasses*, there is a distribution of interstices with different effective coordination numbers, making it very complex to obtain H_r. However, there are reports[20–22] for glasses that show H_r values lower than those calculated from vacancy migration in crystals. In summary, the H_r values for glasses generally fall between 0.1 and 1 and are usually around 0.3 when the molar concentration of the mobile ion is higher than 10%.[21,22] For soda-lime glass, the Haven ratio measured by Mehrer *et al.*[20] is about 0.45 and is practically independent of the temperature.

The *diffusion coefficient for viscous flow* (D_η) can be estimated by the Eyring equation, Eq. (10), where the jump distance d of the moving unit is taken into account. What is commonly done in the literature—and also here—is to assume that $d = d_0$ (d_0 was defined in Subsection II B),

$$D_\eta = \frac{k_B T}{d\eta}. \qquad (10)$$

In Eq. (10), η is the equilibrium viscosity of the liquid. In this paper, we used the MYEGA equation, Eq. (11),[23] to obtain an expression for η as a function of temperature. This equation has three adjustable parameters (η_∞, $T_{g,12}$, and m) that are defined below:

$$\log_{10}(\eta) = \log_{10}(\eta_\infty) + (12 - \log_{10}(\eta_\infty)) \frac{T_{g,12}}{T}$$
$$\times \exp\left[\left(\frac{m}{12 - \log_{10}(\eta_\infty)} - 1\right)\left(\frac{T_{g,12}}{T} - 1\right)\right], \quad (11)$$

$$\eta_\infty \equiv \lim_{T \to \infty} \eta(T), \qquad (12)$$

$$\eta(T_{g,12}) \equiv 10^{12} \text{ Pa} \cdot \text{s}, \qquad (13)$$

$$m \equiv \left.\frac{d\log_{10}(\eta(T))}{d\frac{T_{g,12}}{T}}\right|_{T=T_{g,12}}. \qquad (14)$$

In the equations above, m is the fragility index[24] and $T_{g,12}$ is the temperature where the viscosity is 10^{12} Pa s.

Finally, the *diffusion coefficient for crystal growth* (D_U) is part of Eq. (1). If all the other parameters are known or can be calculated, then D_U can be readily obtained from experimental crystal growth rate data.

III. MATERIALS AND METHODS

A. Glass making

The process of making a stoichiometric lead metasilicate glass was repeated six times trying different homogenization and melting routes in order to produce reproducible, homogeneous samples. One problem with this particular composition is that lead, which is significantly heavier than silicon, tends to accumulate at the bottom of the crucible during the melting procedure. Another is lead evaporation due to its high vapor pressure. These difficulties may result in a chemically inhomogeneous glass, which could be an issue because, in that case, the crystallization kinetics measured in different specimens would not be coherent. Here we report data for two reliable lead metasilicate glasses we made, named *Batch* 1 and *Batch* 2. We distinguish these two glasses even though both yielded similar crystal growth rates, which are also comparable to reported literature data.

The glass of *Batch* 1 was obtained from a mixture of ground quartz SiO_2 (Vitrovita, Brazil) and Pb_3O_4 (Sigma-Aldrich, USA), both of analytical grade, in the required stoichiometric quantities to form $PbSiO_3 + O_2$. 100 g of the powder mixture was thoroughly homogenized in a TURBULA T10B mixer. The homogenous mixture was melted in a Joule effect furnace in a platinum crucible with constant manual agitation with a platinum blade. The temperature did not exceed 1273 K. The melting process took less than 10 min to minimize volatilization of the lead. We just waited until the majority of the bubbles were eliminated, then the melts were poured on a stainless steel plate and pressed with a stainless steel piston to quench them.

The glass of *Batch* 2 was also prepared by melting a thoroughly mixed homogeneous mixture of the same chemicals in a platinum crucible. The melting temperature was 1173 K, with a hold time of 2 h. The melt was then cast between two cold steel plates, resulting in a yellowish glass, similar to that of Batch 1.

B. Viscosity measurements

The viscosity for glass samples of *Batch* 1 was measured in the temperature range of 964–752 K at the Institute of Silicate Chemistry, Russian Federation. The penetration viscosimeter was designed, constructed, and operated by the late Dr. Valentin P. Klyuev. The description of the apparatus can be found elsewhere.[25] We also considered viscosity values reported by different authors,[26–30] including (very rare) isostructural viscosity below T_g reported by Koide *et al.*[30] Isostructural viscosity, as the name suggests, is a measure of viscous flow in a condition for which the structure of the

material does not change during the time scale of the measurements. For more information on this topic, please refer to Ref. 31.

C. Crystal growth rate measurements

We used $2 \times 2 \times 2$ mm^3 samples with polished faces to measure the sizes of the PS crystals as a function of the heat treatment time in isothermal conditions. We used vertical furnaces for the heat treatments and measured the temperatures with a type K thermocouple calibrated following the ASTM E 207–00 standard. We observed the surface crystals and took digital micrographs using a Leica DMRX optical microscope with a Leica DFC490 image acquisition camera.

The time required to nucleate the first crystals on the sample surface at temperatures equal to or lower than 725 K was quite large. Because of that, for these temperatures ($T \leq 725$ K), we "seeded" the sample surface by pre-forming some crystals at 785 K for 34 min. This treatment was enough to nucleate a few crystals that would later grow at the desired growth temperatures. All the image analyses were done with the free and open-source software *ImageJ*.[32] Most of the PS crystals have an ellipsoidal habit; hence, we measured the growth rates of the fastest (longest) crystalline direction. The chosen crystals were isolated in the glassy phase. At each temperature, a unique crystal was located and measured after each heat treatment. The size (half of the longest length of the chosen crystal) *versus* time plots for all the crystals at all temperatures were well described by a linear regression. We also observed spherulitic crystal forms in samples treated at higher temperatures.

We corrected all crystal growth rate data analyzed in this work by the increased liquid–crystal interface temperature using Eq. (15). This important correction is needed because the latent heat released due to crystallization can significantly increase the interface temperature if it is not dissipated fast enough. Herron and Bergeron[33] measured the temperature increase at the liquid–crystal interface during the crystal growth process in several oxide glass-formers. Cassar[19] reanalyzed their data and obtained the following empirical expression:

$$\Delta T_i (T) = 10^{0.64} (U (T) \Delta H_m)^{0.58}, \tag{15}$$

where ΔT_i is the liquid–crystal interface temperature increase at a temperature T. In this expression, U is given in m/s and ΔH_m in J/mol.

D. Impedance measurements

The ionic conductivity of samples of *Batch* 1 was obtained via electrochemical impedance spectroscopy (EIS). For EIS measurements, gold was sputtered on parallel opposite faces of a glass specimen in order to ensure electrical contact. The sample was 0.294 cm thick and had a contact area of 0.602 cm^2. EIS measurements were conducted using a Novocontrol Alpha-A impedance analyzer over the frequency range 10 MHz–0.1 Hz, with an applied root mean square AC voltage of 500 mV. These measurements were carried out at temperatures below T_g over the range of 473–673 K. The temperature

control was performed by using the Novotherm temperature control system with maximum temperature variation of ±0.1 K (if the variation is higher than 0.1 K, the equipment stops the measurement, waits for stabilization, and then returns to the measurement) during the EIS measurements.

To determine the ionic conductivity σ of PbSiO$_3$ glass, we fitted the impedance data using *Zview* 3.5 and an appropriate equivalent circuit. The chosen equivalent circuit [shown in Fig. 2(a)] comprises a parallel combination of a resistance (R_g) and a constant phase element (CPE$_g$) taking into account the glass sample resistance and capacitance, in series with a CPE$_e$ related to electrode polarization (blocking ion effect). The used type of data weighting was calc-modulus since the obtained impedance spectrum covers a wide range of impedances.[34]

E. Activation energy

We computed the activation energies, E, for three diffusional processes—crystal growth (below the decoupling temperature T_d), lead diffusion, and isostructural viscosity—by fitting an Arrhenian expression,

$$D (T) = D_0 \exp\left(-\frac{E}{RT}\right), \tag{16}$$

where D is the diffusion coefficient and D_0 is a constant.

We obtained E using a robust linear regression on a linearized plot of $\ln (D)$ *versus* $1/RT$. The uncertainty was obtained considering a confidence level of 95%. The algorithm used was the function "theilslope"[35] that implements a Theil–Sen estimator.[36,37] This algorithm is available in the free and open-source SciPy module[38] for the Python programming language.

The effective activation energy for equilibrium viscosity depends on the temperature, and we obtained it by using Eq. (17).[39] In this equation, we used the MYEGA regression [Eq. (11)] for $\log_{10} (\eta (T))$,

$$E_{\eta,\text{eff}} (T) = R \ln (10) \frac{d \log_{10} (\eta (T))}{d 1/T}. \tag{17}$$

IV. RESULTS AND DISCUSSION

A. Ionic conductivity

Figure 1 shows the dependence of the real (Z') and imaginary ($-Z''$) parts of impedance as a function of frequency over a range of temperatures (473–673 K), measured for samples of *Batch* 1. The inverse of electrical conductivity can be promptly read on the left y axis at the low frequency plateau because the results were normalized by the shape factor of the sample (thickness over area). The dependence of electrical conductivity with temperature is logarithmic, as expected.

With respect to the imaginary part of impedance, the $-Z''$ peak shifts to higher frequencies as the temperature is increased, since the relaxation frequency is increasing as the bulk resistance R_g of the glass decreases ($f \sim 1/R_g C$, C is the capacitance). The most important result is that at higher temperatures (633–673 K)—where the used frequency range can cover the entire electrical behavior of the cell Au/Glass/Au—the $-Z''$ part starts to increase again in low frequencies. This
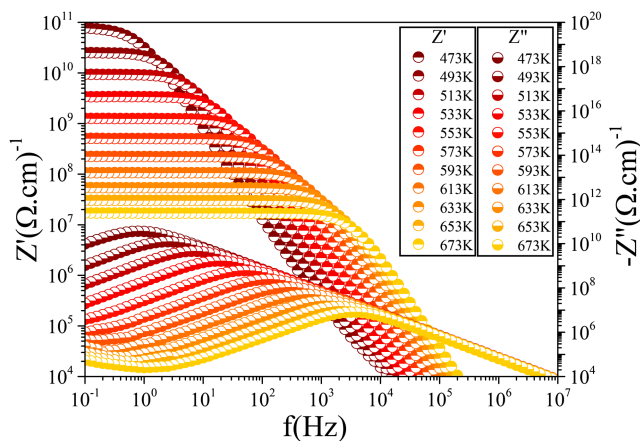
FIG. 1. Dependence of the real (half up filled symbol) and imaginary (half down filled symbol) parts of impedance on frequency, normalized by the shape factor.

behavior is typical for an ion conductor, and it is caused by a blocking ion effect in the metallic electrode.

Conversely, in case of an electronic conductor, $-Z''$ should decrease continuously, since the electrode used in the measurement (gold in this case) is several orders of magnitude more conductive than the analyzed glass. On the other hand, the blocking ion effect occurs because the ions cannot pass through the electrode used. These results indicated that the resistivity measured here takes place by the motion of ions through the glass, most likely Pb^{2+}. Indeed, Cohen *et al.*[40] already reported a similar result when they measured the resistivity of a $PbSiO_3$ glass, and their results were in close agreement with published data for Pb-ion diffusion.[40]

Figure 2(a) shows the complex impedance and the fitted curves. The glass capacitances C ranged between 2 and 3 pF, resulting in a dielectric constant (ε_r) between 23 and 33, which is in good agreement with the expected dielectric constant for this type of material.[40] The electrode capacitances, which were determined only at higher temperatures (633–673 K), ranged from 1 to 12 μF. At lower temperatures, the used frequency range could not cover the entire electrical behavior of the Au/Glass/Au cell; therefore, there is no electrode response.

We estimated a theoretical electrode capacitance of 4.4 μF by considering a monolayer of Pb^{2+} ions of ionic radius of

119 pm blocked at both sides of the electrode and using the electrode area of the glass sample (0.6 cm^2) and a reasonable $\varepsilon_r \sim 2$ (this procedure is the same as discussed in Ref. 41). This result is in agreement with the experimental electrode capacitances that we obtained, supporting that the electrical conductivity of the PS glass is caused mainly by Pb^{2+} motion.

In addition, we calculated the activation energy (E_a) for Pb ion conduction using an Arrhenius equation [Fig. 2(b)]. The coefficient of determination (R^2), the activation energy (E_a), and pre-exponential term (σ_0) of an Arrhenius-like equation ($\sigma T = \sigma_0 \exp[-E_a/RT]$) are also shown in the plot. The E_a = 1.267(9) eV is in close agreement with previous reported results of 1.12 eV.[40] To obtain D_σ, we used Eq. (9) for the conductivity data. Here we used a N_i of 1.274×10^{28} Pb^{+2}/m^3 estimated by using a density[15] of 6 g/cm^3 and the nominal molar weight of 1:1 $PbSiO_3$ composition. Finally, to obtain D_{Pb}, we used the average value of 0.3 ± 0.2 for H_r (this is the origin of the uncertainty bars in Fig. 6 that will be presented later in the manuscript).

B. Viscosity and crystal growth rates

Figure 3 shows the experimental viscosity data measured in this work (*Batch* 1) together with the literature data over a wide range of temperatures. The agreement between the different datasets is good enough and within the usual viscosity measurement errors. We fitted the MYEGA equation, Eq. (11), to all these data (except Koide's isostructural viscosity[30]) and obtained $T_{g,12}$ = 679.9(3) K, m = 55.1(4), and $\log_{10}(\eta_\infty)$ = −1.76(6) (η_∞ in Pa s, the uncertainty is one standard deviation, computed by the regression algorithm). We then used the fitted viscosity curve in all of the following calculations.

Crystal growth rate data for lead metasilicate glasses between 723 and 998 K have been reported by Neiman *et al.*[42] Figure 4 shows the crystal growth rates obtained in this work plotted together with the aforementioned data. This combined dataset spans six orders of magnitude, between 10^{-6} and 10^{-12} m/s. In particular, the maximum growth rate was observed at about 923 K ($T_{max}/T_m \sim 0.90$). Hence, we have significantly extended the temperature range of available experimental crystal growth rates for this composition
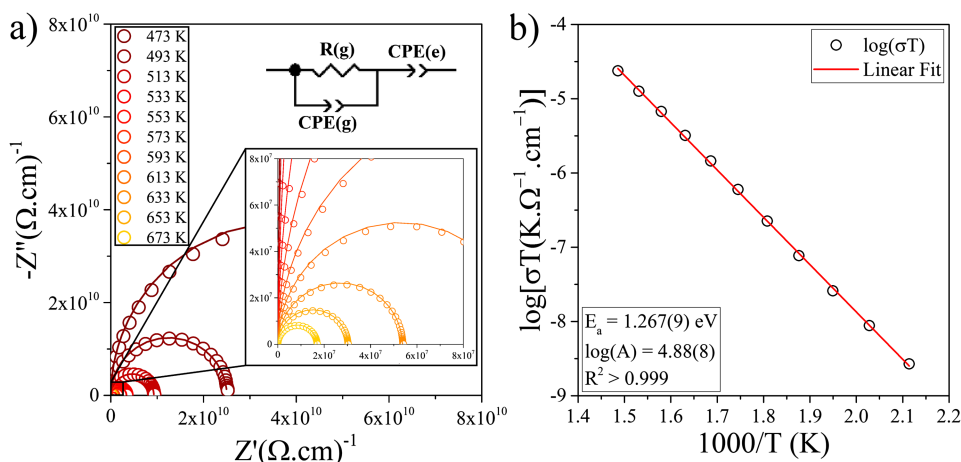

FIG. 2. Set of EIS analyses represented by (a) complex impedance plots of a PS glass sample in the temperature range of 473–673 K (symbols) and their respective fit (line) based on the shown equivalent circuit and (b) the Arrhenius plot for the dependence of ionic conductivity on inverse temperature.
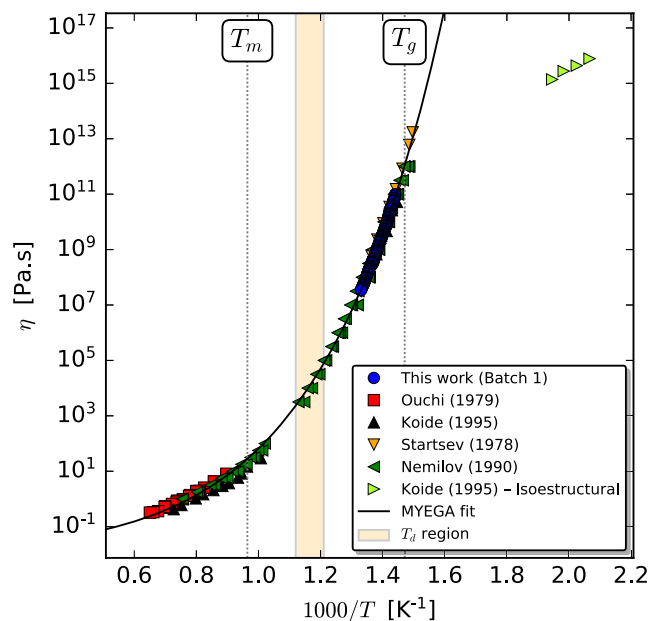
FIG. 3. Equilibrium and non-equilibrium viscosity data for samples from Batch 1 combined with selected datasets obtained by different techniques for different batches of lead metasilicate glasses reported by different authors.[26–30] The full line is a regression of all these data points using the MYEGA equation.[23] The T_d region will be discussed in the text.

toward the glass transition range. The ellipsoid shaped surface crystals that nucleate in this composition are shown in Fig. 5.

Figure 4 shows two calculated crystal growth rate curves considering the *Secondary Superficial Nucleation* growth model. The full line is for the layer-by-layer case, for which we used a value of 32 Å for d_0 and 0.97 mJ/m^2 for γ. The traced line is for the polynuclei case with $d_0 = 11$ Å and $\gamma = 13$ mJ/m^2.
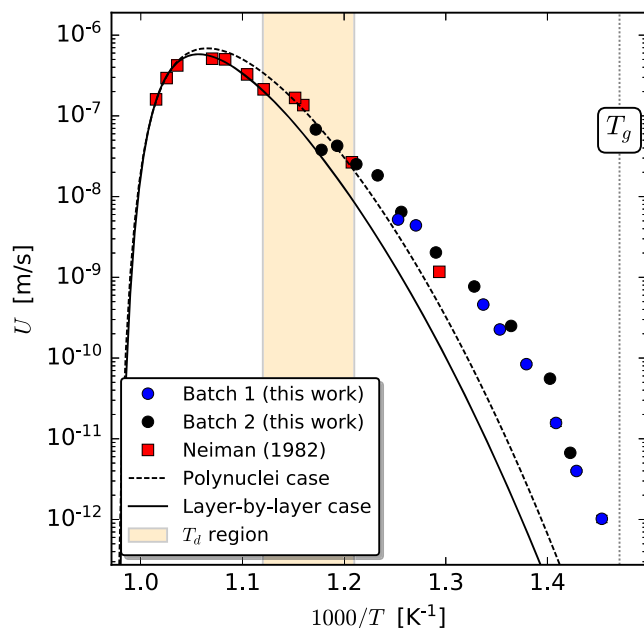

FIG. 4. Crystal growth rates measured for samples of the two studied batches together with data from Neiman *et al.*[42] The two fitted curves are based on the 2D growth model, which satisfactorily describes the high temperature data. The uncertainty bars for our data are smaller than the symbol size. The T_d region is discussed in the text.
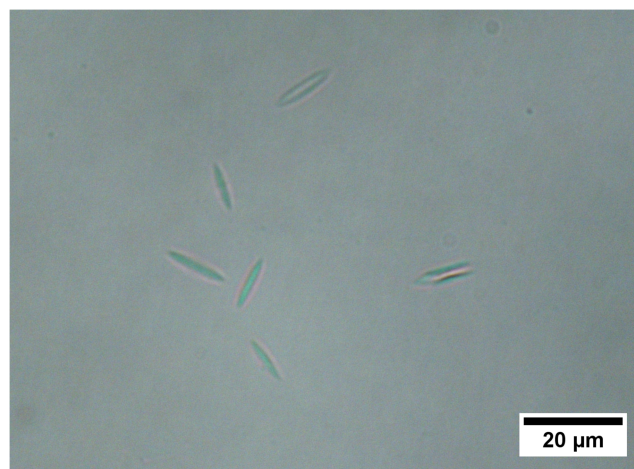

FIG. 5. Surface of a PS glass sample (*Batch* 1) heat treated at 785 K observed by optical microscopy with transmitted light using 50 × objective lenses.

These values are those that best fit the data. Only the data near the melting point could be successfully fitted. We found no combination of these two parameters that satisfactorily fitted the data to temperatures below 807 K.

The values for d_0 are of the expected order of magnitude (i.e., the size of a few unit cells), but the values for γ are much lower than those reported for primary crystal nucleation studies (which are usually in the range of 100–200 mJ/m^2 for silicate glasses). This, however, is not an issue. For instance, Calvert and Uhlmann[43] studied the difference between the γ value for primary crystal nucleation and for secondary-nucleation driven crystal growth and also found that the latter is smaller. In their manuscript, they analyzed crystallization data for five compositions and systematically obtained values for γ from growth mediated by secondary superficial crystal nucleation that are typically one order of magnitude lower (i.e., ~10 mJ/m^2) than those for primary crystal nucleation. This is in good agreement with the value for γ that we obtained here for the polynuclei case. In any case, the values for d_0 and γ in our analysis are only approximations because all the uncertainties of the used parameters and experimental data—as well as the uncertainties due to the assumptions of the model—are accumulated in these two unconstrained parameters.

It is important to state that two other popular crystal growth models—the *screw dislocation* and the *normal* growth model[16]—were not able to fit the high temperature data reasonably well, even with these two free parameters (d_0 and γ). Another interesting detail is that Neiman measured the growth of the crystalline layer, whereas we measured crystals growing on the glass surface. Even with this difference, both datasets are in very good agreement in the temperature range where they overlap.

Figure 4 shows that even the considered model (Secondary Superficial Nucleation growth) was not sufficient to describe the crystal growth data in the whole temperature range. This finding supports the well-known concept that this supercooled liquid also undergoes the classical decoupling between crystal growth kinetics and viscous flow at a certain temperature above T_g. Previous data hinted that this could be the case for this

material, but now, with our extended growth data, the overall picture is much clearer. In some figures, we delimited a "T_d region." This is the temperature range where the crystal growth decouples from viscous flow. That is, below this temperature range they are decoupled. We estimated the T_d region as being in the range of $807 \leq T \leq 893$ K ($1.2 T_g$–$1.3 T_g$).

Our analysis is in agreement with a previous test for the decoupling done by Nascimento *et al.*, considering much less data points.[3] This, however, is *not* the most important finding of this article; we are more interested in calculating the diffusivities controlling viscous flow and crystal growth and comparing them with those of the individual elements.

C. Diffusion coefficients

The dynamic properties presented above are controlled and connected to diffusion processes and provide a unique opportunity for performing a comparative analysis to estimate the effective diffusion coefficients that control viscous flow and crystallization. To boost this analysis, we used additional data on the ionic conductivity and self-diffusion coefficients of the cationic species Si^{4+} and Pb^{2+}, which were measured in actual diffusion experiments and also by electrochemical impedance spectroscopy.

Figure 6 summarizes all the different diffusivities measured or calculated in a wide temperature range from above the melting point to below the glass transition range. It is important to note that they include viscous flow and crystal growth measurements from different authors in a wide temperature interval. To the best of our knowledge, this study comprises one of the most complete sets of diffusion processes ever collected, calculated, and analyzed for an oxide glass-forming system. It covers four different transport processes spanning

TABLE I. Activation energies for the diffusion processes studied here. A mole here is defined as a mole of $PbSiO_3$.

Symbol	Diffusion process	ΔT range (K)	Activation energy (kJ/mol)	Reference for data
$E_{Pb,1}$	Pb self-diffusion (Batch 1)	473–673	117(2)	This study
$E_{Pb,2}$	Pb self-diffusion	613–807[a]	100(20)	44
E_{iso}	Isostructural viscosity	484–514	120(40)	30
$E_{\eta,eff}$	Equilibrium viscosity	646–1537	Figure 7	This study and Refs. 26–30
$E_{U,1}$	Crystal growth (Batch 1)	688–798	370(90)	This study
$E_{U,2}$	Crystal growth (Batch 2)	703–807[a]	260(30)	This study

[a]The upper temperature limit was chosen to avoid data in the T_d region [see Fig. 6(a)].

16 orders of magnitude in a wide range of temperatures, from above T_m to far below T_g! We believe that these plots can give a thought-provoking insight into the diffusion kinetics in this non-crystalline material.

D. Activation energy

Table I compiles the activation energy for all the diffusion processes studied here, together with the temperature range where the computation was performed. For some calculations, we limited the range to allow only data *below* the T_d region. These are marked with the letter "a" in the table. The reasoning for this is that, for temperatures in the T_d region and above, the viscosity starts to control these processes, which results in a deviation from an Arrhenian behavior showing a temperature dependence of the activation energy.

The data of Table I readily show that $E_{Pb,1}$ is statistically equal to $E_{Pb,2}$ (within the uncertainty), which is expected and
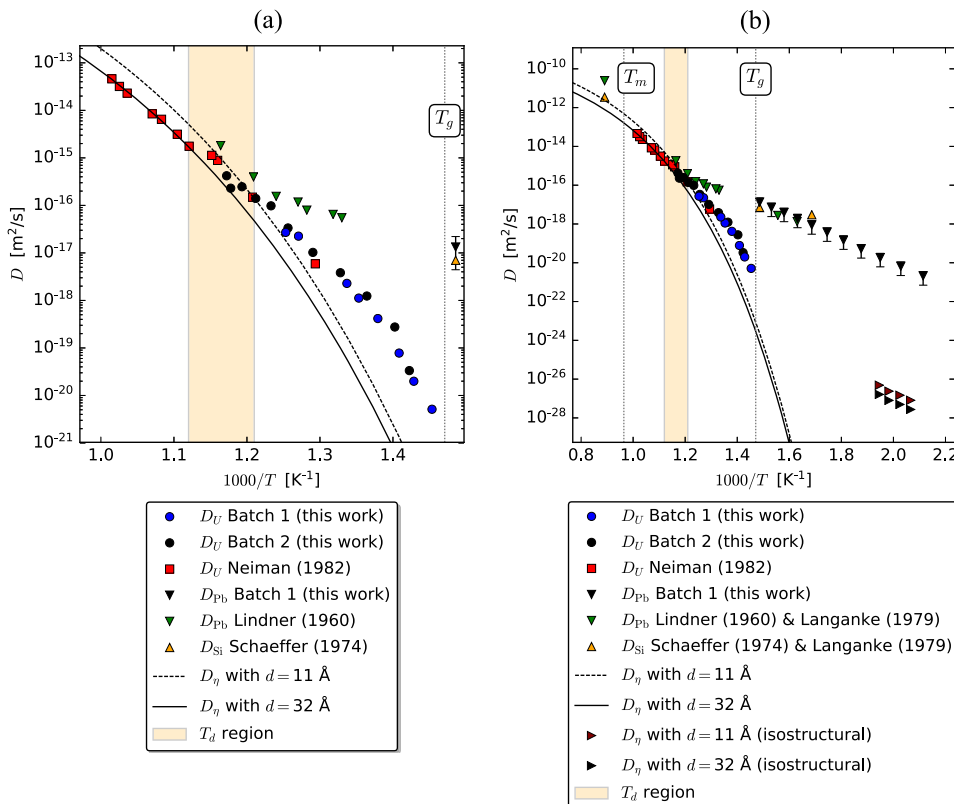

FIG. 6. Temperature dependence of the effective diffusion coefficients calculated from crystal growth rates and viscosity, and measured ionic conductivity, as well as self-diffusion coefficients of Si and Pb. (a) Zoom in the temperature range where crystal growth data are available. (b) Overall picture that spans 16 orders of magnitude.
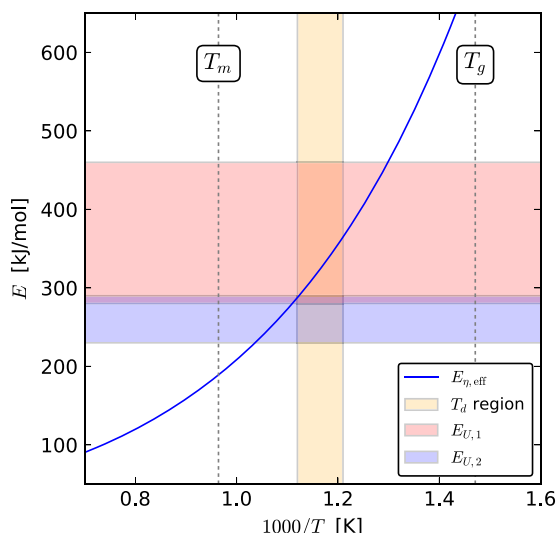
FIG. 7. Effective activation energy for equilibrium viscosity as a function of temperature plotted with the values for $E_{U,1}$ and $E_{U,2}$ (see Table I).

FIG. 8. D_U/D_η and D_{Pb}/D_η against the inverse of temperature. Observe the gradual deviation from the $D_U = D_\eta$ full line, showing the decoupling between crystal growth and viscous flow.

suggests that there is no mechanism change in lead diffusion from 473 up to 807 K. What is quite interesting is that lead diffusion has the same activation energy as the isostructural viscosity, E_{iso}. This result suggests that the mechanism that controls non-equilibrium viscous flow is the same that controls Pb ionic diffusion.

The magnitude of lead and silicon diffusivities below T_g is quite similar. Unfortunately, the scarcity of data for silicon diffusion below the T_d region inhibits a more detailed analysis. It is known that lead (partially) and silicon (always) have the role of glass-formers[40] in this particular system, and this fact would suggest that their diffusivities could be close. In addition, Schaeffer[10] suggested that the oxygen self-diffusion has the same order of magnitude as that of silicon in most silicate glasses, which could indicate a possible mechanism of diffusion by cooperation of these 3 species.

Finally, the activation energies for crystal growth measured in samples of two batches, $E_{U,1}$ and $E_{U,2}$, are statistically equal. Moreover, they are comparable to the effective activation energy for viscous flow in the T_d region, as shown in Fig. 7. This observation may be particular to this specific composition, but we believe it might be useful to connect $E_{\eta,eff}(T_d)$ with E_U. This, however, is not in the scope of the present study.

E. Decoupling

Figure 8 complements our analyses by showing the ratio D_U/D_η and D_{Pb}/D_η as a function of the inverse temperature. Looking at Fig. 6(a), one might think that the crystal growth data below the decoupling temperature are somewhat parallel to the viscosity, suggesting that there is actually *no* decoupling; perhaps only a change of growth mechanism that resulted in a shift of D_U. Visually this may seem to be the case, but Fig. 8 shows that it is not. If the curves were parallel, then the D_U/D_η data would reach a *plateau* at some temperature below the decoupling. A glimpse at Fig. 8 clearly shows that this does not happen.
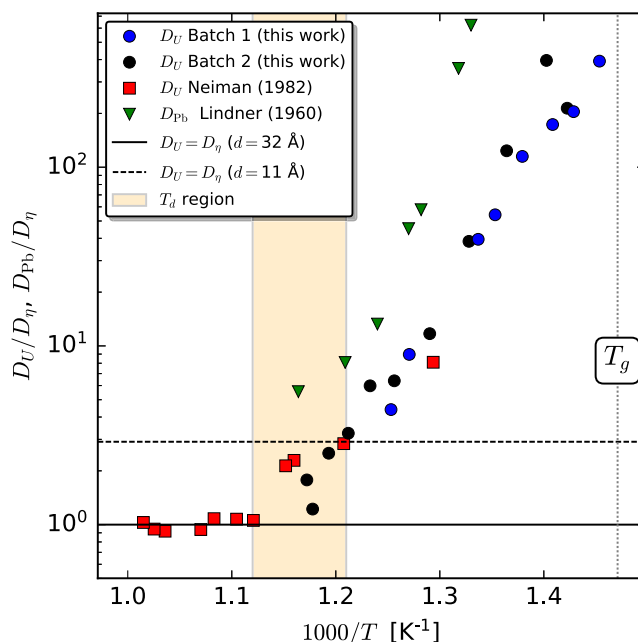
Lindner[44] also pointed out that there was a sharp change in the lead diffusion coefficient at 806 K, showing two straight lines, suggesting a transition of the diffusion mechanism due to two widely different activation energies. This could be seen as additional evidence for the decoupling, observed from diffusion experiments. It is interesting that lead diffusivity seems to decouple from viscous flow in the same temperature range where crystal growth and viscosity decouple.

F. Diffusing entities

The calculated values of D_{Pb} from conductivity data closely agree with the reported lead diffusivities, suggesting that electrical conduction in lead metasilicate glasses takes place mainly by the motion of Pb^{2+} ions. Moreover, silicon diffusion is clearly decoupled from viscous flow at lower temperatures, as shown in Fig. 6(b). It is hard to draw a conclusion about silicon diffusion above the melting temperature because only one data point is available. However, it is worth mentioning that it is within an order of magnitude of that of viscous flow diffusion.

We believe that this combined dataset gives a stimulating insight into the microscopic nature of the diffusion processes controlling crystal growth and viscous flow for this oxide glass-former and may be a good basis for further detailed studies of kinetic phenomena. In the following paragraphs, we discuss our hypothesis about the diffusing entities that control the studied kinetic processes in $PbSiO_3$.

At *temperatures above the T_d range* (i.e., above 893 K), viscous flow and crystal growth kinetics are coupled and they both seem to be limited by the mobility of the network forming cations (Si and Pb). In other words, they are governed by the same mechanism. This means that D_U, D_η, D_{Si}, and D_{Pb} are proportional to each other (activation energies are quite

similar). This finding provides further evidence to support the validity of the Eyring equation for temperatures that are sufficiently high, in agreement with previous studies in other silicate systems.[3,45]

At *temperatures below the T_d range* (i.e., below 807 K), the diffusivities controlling viscous flow and crystal growth are clearly different characterizing the classical decoupling phenomenon, which has been assigned by different authors to *dynamic heterogeneities.*[46,47] The Eyring equation no longer predicts crystal growth dynamics, and at least three different diffusing entities seem to be present: one that controls the equilibrium viscosity (slowest), one that controls crystal growth (intermediate), and one that controls self-diffusion of the network forming ions, and perhaps also non-equilibrium viscosity (fastest). Hence, our results show that at deep supercoolings, the viscous flow and crystal growth kinetics are controlled by different diffusion entities. In addition, individual network formers (Si and Pb) have a much faster diffusivity, and their activation energy is very similar to that of non-equilibrium viscosity.

The overall results suggest that, below the decoupling temperature, both viscous flow and crystal growth indeed require a cooperative movement of some "structural units" or "molecules" instead of just jumps of one or a few isolated atoms. However, these units have different chemical natures or sizes for these two dynamic processes, resulting in different activation energies. This is the most original and relevant finding of this research work.

V. SUMMARY AND CONCLUSIONS

We studied the diffusion coefficients controlling four different dynamic processes in a liquid, supercooled liquid, and glass with $PbSiO_3$ composition: crystal growth rates, equilibrium viscosity, non-equilibrium viscosity, and cationic self-diffusion of Si and Pb. With this extensive dataset, we searched for clues that could shed light on the mechanism underlying the well-known decoupling between crystal growth and viscous flow.

Based on our results, we propose that the nature and/or size of the diffusing units that control viscous flow are *different* from the diffusing units that control crystal growth *and* they are not single cations (lead or silicon), but some slower (larger) structural units. On the other hand, at temperatures above T_d, crystal growth and viscosity are controlled by the same diffusing units.

Another interesting result is that lead diffusion below T_d has the same activation energy as isostructural viscosity, suggesting that the latter is controlled by lead atom hopping.

Taken *in toto*, these findings shed some light on the understanding of transport properties, such as crystallization, self-diffusion, and viscous flow in liquid and glassy $PbSiO_3$, and

may be useful for further studies with other glass-forming systems.

SUPPLEMENTARY MATERIAL

See supplementary material for the experimental data obtained from this study in table format.

APPENDIX: AN EXPRESSION FOR A_0

The parameter A_0 present in Eq. (2) is the critical area to form a secondary nucleus at the crystal–ambient interface. Figure 9 illustrates the secondary nucleation. When a secondary nucleus with cylindrical shape nucleates, it has a volume V_c,

$$V_c(r) = \pi r^2 h, \tag{A1}$$

and it creates the additional area A_c (shown in gray in Fig. 9),

$$A_c(r) = 2\pi r h. \tag{A2}$$

The change in the Gibbs free energy (ΔG_c) due to the nucleation of a secondary nucleus is

$$\Delta G_c(r, T) = V_c(r)\Delta G_V(T) + A_c(r)\gamma. \tag{A3}$$

Taking the partial derivative of ΔG_c in respect of r, we obtain

$$\frac{\partial \Delta G_c(r, T)}{\partial r} = 2\pi h r \Delta G_V(T) + 2\pi h \gamma. \tag{A4}$$

The critical radius, r_{2D}^*, is the radius where Eq. (A4) is zero. It means that any increase in the radius above this critical value will result in a decrease in the Gibbs free energy.

$$\left.\frac{\partial \Delta G_c(r, T)}{\partial r}\right|_{r=r_{2D}^*} = 2\pi h r_{2D}^* \Delta G_V(T) + 2\pi h \gamma = 0. \tag{A5}$$

Rearranging the above expression and using the relation[18] $\Delta\mu_V = -\Delta G_V$, we have

$$r_{2D}^*(T) = \frac{\gamma}{\Delta\mu_V(T)}. \tag{A6}$$

Substituting Eq. (A6) in Eq. (A2) and considering that $h = d_0$, we have an expression for A_0,

$$A_c\left(r_{2D}^*(T)\right) \equiv A_0(T) = \frac{2\pi d_0 \gamma}{\Delta\mu_V(T)}. \tag{A7}$$
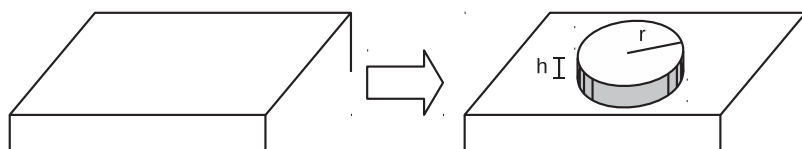

FIG. 9. Schematics of the nucleation of a secondary nucleus.

[1] S. Glasstone, K. J. Laidler, and H. Eyring, *The Theory of Rate Processes: The Kinetics of Chemical Reactions, Viscosity, Diffusion and Electrochemical Phenomena* (McGraw-Hill Book Company, Inc., 1941).

[2] M. D. Ediger, P. Harrowell, and L. Yu, J. Chem. Phys. **128**, 034709 (2008).

[3] M. L. F. Nascimento and E. D. Zanotto, J. Chem. Phys. **133**, 174701 (2010).

[4] M. L. F. Nascimento and E. D. Zanotto, Phys. Rev. B **73**, 024209 (2006).

[5] I. Farnan and J. F. Stebbins, Science **265**, 1206 (1994).

[6] I. Farnan, Curr. Opin. Solid State Mater. Sci. **3**, 371 (1998).

[7] J. F. Stebbins, Am. Mineral. **101**, 753 (2016).

[8] B. Langanke and H. Schmalzried, Ber. Bunsengesellschaft Phys. Chem. **83**, 59 (1979).

[9] R. Lindner, W. Hassenteufel, and Y. Kotera, Z. Phys. Chem. **23**, 408 (1960).

[10] H. A. Schaeffer, Phys. Status Solidi A **22**, 281 (1974).

[11] D. De Sousa Meneses, M. Malki, and P. Echegut, J. Non-Cryst. Solids **352**, 769 (2006).

[12] S. Feller, G. Lodden, A. Riley, T. Edwards, J. Croskrey, A. Schue, D. Liss, D. Stentz, S. Blair, M. Kelley, G. Smith, S. Singleton, M. Affatigato, D. Holland, M. E. Smith, E. I. Kamitsos, C. P. E. Varsamis, and E. Ioannou, J. Non-Cryst. Solids **356**, 304 (2010).

[13] J. Schneider, V. R. Mastelaro, E. D. Zanotto, B. A. Shakhmatkin, N. M. Vedishcheva, A. C. Wright, and H. Panepucci, J. Non-Cryst. Solids **325**, 164 (2003).

[14] S. K. Lee and E. J. Kim, J. Phys. Chem. C **119**, 748 (2015).

[15] S. Kohara, H. Ohno, M. Takata, T. Usuki, H. Morita, K. Suzuya, J. Akola, and L. Pusztai, Phys. Rev. B **82**, 134209 (2010).

[16] I. S. Gutzow and J. W. P. Schmelzer, *The Vitreous State: Thermodynamics, Structure, Rheology, and Crystallization* (Springer, London, 2013).

[17] K. F. Kelton, in *Solid State Physics*, edited by H. Ehrenreich and D. Turnbull (Academic Press, Berlin, 1991), pp. 75–177.

[18] D. R. Cassar, Int. J. Appl. Glass Sci. **7**, 262 (2016).

[19] D. R. Cassar, "Crystal nucleation, growth, relaxation and viscous flow in diopside and lithium diborate glasses," Ph.D. thesis, Universidade Federal de São Carlos, 2014.

[20] H. Mehrer, A. W. Imre, and E. Tanguep-Nijokep, J. Phys.: Conf. Ser. **106**, 012001 (2008).

[21] J. O. Isard, J. Non-Cryst. Solids **246**, 16 (1999).

[22] E. Bychkov, D. L. Price, and A. Lapp, J. Non-Cryst. Solids **293-295**, 211 (2001).

[23] J. C. Mauro, Y. Yue, A. J. Ellison, P. K. Gupta, and D. C. Allan, Proc. Natl. Acad. Sci. U. S. A. **106**, 19780 (2009).

[24] C. A. Angell, in *Relaxation in Complex Systems*, edited by K. L. Ngai and G. B. Wright (Naval Research Laboratory, Springfield, 1985), pp. 3–12.

[25] V. P. Klyuev, Glass Phys. Chem. **26**, 559 (2000).

[26] S. Nemilov, Izv. Akad. Nauk SSSR Neorg. Mater. **4**, 952 (1968).

[27] S. Nemilov and A. Ignat'ev, Fiz. Khim. Stekla **16**, 85 (1990).

[28] Y. Ouchi and E. Kato, J. Jpn. Inst. Met. **43**, 625 (1979).

[29] Y. K. Startsev, V. P. Klyuev, and M. S. Vostrikova, Fiz. Khim. Stekla **4**, 278 (1978).

[30] M. Koide, R. Sato, T. Komatsu, and K. Matusita, Phys. Chem. Glasses **36**, 172 (1995).

[31] O. Mazurin, Y. Startsev, and S. Stoljar, J. Non-Cryst. Solids **52**, 105 (1982).

[32] C. A. Schneider, W. S. Rasband, and K. W. Eliceiri, Nat. Methods **9**, 671 (2012).

[33] L. W. Herron and C. G. Bergeron, Phys. Chem. Glasses: Eur. J. Glass Sci. Technol., Part B **19**, 89 (1978).

[34] *Impedance Spectroscopy: Theory, Experiment, and Applications*, edited by E. Barsoukov and J. R. Macdonald, 2nd ed. (Wiley-Interscience, Hoboken, NJ, 2005).

[35] scipy.stats.theilslopes — SciPy v0.15.1 Reference Guide, available at https://docs.scipy.org/doc/scipy-0.15.1/reference/generated/scipy.stats.theil slopes.html.

[36] H. Theil, in *Henri Theil's Contributions to Economics and Econometrics*, edited by B. Raj and J. Koerts (Springer, Netherlands, Dordrecht, 1992), pp. 345–381.

[37] P. K. Sen, J. Am. Stat. Assoc. **63**, 1379 (1968).

[38] T. E. Oliphant, Comput. Sci. Eng. **9**, 10 (2007).

[39] J. W. P. Schmelzer, A. S. Abyzov, V. M. Fokin, C. Schick, and E. D. Zanotto, J. Non-Cryst. Solids **428**, 68 (2015).

[40] B. M. Cohen, D. R. Uhlmann, and R. R. Shaw, J. Non-Cryst. Solids **12**, 177 (1973).

[41] *Solid State Electrochemistry*, edited by P. G. Bruce, 1st ed. (Cambridge University Press, Cambridge, 1997).

[42] T. Neiman, H. Yinnon, and D. R. Uhlmann, J. Non-Cryst. Solids **48**, 393 (1982).

[43] P. D. Calvert and D. R. Uhlmann, J. Cryst. Growth **12**, 291 (1972).

[44] R. Lindner, Acta Chem. Scand. **5**, 735 (1951).

[45] M. L. F. Nascimento, V. M. Fokin, E. D. Zanotto, and A. S. Abyzov, J. Chem. Phys. **135**, 194703 (2011).

[46] H. Sillescu, J. Non-Cryst. Solids **243**, 81 (1999).

[47] M. D. Ediger, Annu. Rev. Phys. Chem. **51**, 99 (2000).